Recyclable CRISPR/Cas9 mediated gene disruption and deletions in *Histoplasma*

Bastian Joehnk[1]*, Nebat Ali[1], Mark Voorhies[1], Keith Walcott[1], Anita Sil[1,2#]

[1]Department of Microbiology and Immunology, University of California San Francisco, San Francisco, California, USA

[2]Chan Zuckerberg Biohub – San Francisco, San Francisco, CA 94158

*Current address: Bastian Joehnk, Formo Bio GmbH, Frankfurt am Main, Germany

#Address correspondence to Anita Sil, anita.sil@ucsf.edu.

Running Head: Recyclable CRISPR system for *Histoplasma* gene editing

Abstract

Targeted gene disruption is challenging in the dimorphic fungal pathogen *Histoplasma* due to the low frequency of homologous recombination. Transformed DNA is either integrated ectopically into the genome or maintained extra chromosomally by ~~the~~ *de novo* addition of telomeric sequences. Based on a system developed in *Blastomyces*, we adapted a CRISPR/Cas9 system to facilitate targeted gene disruption in *Histoplasma* with high efficiency. We express a codon-optimized version of Cas9 as well as guide RNAs from a single ectopic vector carrying a selectable marker. Once the desired mutation is verified, one can screen for isolates that have lost the Cas9 vector by simply removing the selective pressure. Multiple mutations can then be generated in the same strain by retransforming the Cas9 vector carrying different guides. We used this system to disrupt a number of target genes including *RYP2* and *SRE1* where loss-of-function mutations could be monitored visually by colony morphology or color, respectively. Interestingly, expression of two guide RNAs targeting the 5' and 3' ends of a gene allowed isolation of deletion mutants where the sequence between the guide RNAs was removed from the genome. Whole-genome sequencing showed that the frequency of off-target mutations associated with the Cas9 nuclease was negligible. Finally, we increased the frequency of gene disruption by using an endogenous *Histoplasma* regulatory sequence to drive guide RNA expression. These tools transform our ability to generate targeted mutations in *Histoplasma*.

Importance

Histoplasma is a primary fungal pathogen with the ability to infect otherwise healthy mammalian hosts, causing systemic and sometimes life-threatening disease. Thus far,

molecular genetic manipulation of this organism has utilized RNA interference, random insertional mutagenesis, and a homologous recombination protocol that is highly variable and often inefficient. Targeted gene manipulations have been challenging due to poor rates of homologous recombination events in *Histoplasma*. Interrogation of the virulence strategies of this organism would be highly accelerated by a means of efficiently generating targeted mutations. We have developed a recyclable CRISPR/Cas9 system that can be used to introduce gene disruptions in *Histoplasma* with high efficiency, thereby allowing disruption of multiple genes.

Introduction

The fungal order Onygenales includes multiple thermally dimorphic mammalian pathogens capable of infecting healthy hosts (1). These organisms include *Histoplasma spp.*, which are the most common cause of fungal respiratory infections in the US. Approximately 60-90% of individuals residing in the Ohio and Mississippi River Valleys are thought to have been exposed to *Histoplasma*, with the disease histoplasmosis reaching an incidence of up to 4.3 cases per 100,000 population in endemic regions and a mortality rate of up to 7% (2, 3). *Histoplasma* grows saprophytically with a filamentous morphology in the soil that generates asexual spores termed macro- and microconidia. These conidia, the infectious agents of *Histoplasma*, are inhaled by mammalian hosts and phagocytosed by alveolar macrophages. Upon the shift to higher body temperature, *Histoplasma* converts to a pathogenic yeast form that expresses virulence factors, enabling proliferation inside the phagolysosome and eventually leading to the lysis of the infected macrophage. Thus, the dimorphic nature of this fungus is thought to be an important pathogenicity factor and is a subject of major interest (4). Several molecular tools have been developed to study morphogenesis, such as genome wide expression studies, genetic screens based on random insertional mutagenesis, and RNA interference. These techniques led to the identification of key players of dimorphic switching such as the Ryp proteins, which are required for yeast phase growth of *Histoplasma*. However, in contrast to the majority of fungal model organisms, gene disruptions or replacements in *Histoplasma* are impeded by its low rate of homologous recombination, making gene targeting challenging (5).

In recent years, CRISPR/Cas9-based genome editing has become a powerful addition to the genetic tool set for molecular research of fungi. CRISPR/Cas9-based systems have been successfully adapted to genetically manipulate yeasts such as *Saccharomyces cerevisiae*, *Pichia pastoris* and *Candida albicans* as well as multiple filamentous fungal species including *Aspergilli*, *Neurospora crassa*, and *Trichoderma reesei* (6-11). More recently, CRISPR/Cas9 tools were developed for the dimorphic fungal pathogen *Blastomyces dermatitidis* (12), a close relative of *Histoplasma*. Notably, most fungal CRISPR/Cas9 based systems rely on one of two delivery systems: i) the transformation of *in vitro* assembled Cas9 sgRNA complexes called ribonucleoproteins (RNPs) or ii) the expression of both Cas9 nuclease and sgRNA within the fungal cell. The transformation of Cas9 sgRNA RNPs is generally simpler as it does not require laborious strain development and has the advantage of being essentially marker free (13). However, this method is not applicable to all species and in fact we could not optimize it for *Histoplasma* (data not shown). In contrast, expression of Cas9 and sgRNAs inside the fungal cell usually requires the genomic integration of the respective expression cassettes. The integration can result in unwanted side effects, such as the disruption of a random gene at the integration site. Furthermore, expression of sgRNAs is usually driven by RNA polymerase III promoters to generate functional non-modified sgRNAs. However, RNA pol III promoters are not well defined in fungi and there is only limited information about their expression kinetics. This problem was circumvented by Nødvig et al. by developing a special expression system for the sgRNA, which utilizes a well-defined constitutive RNA polymerase II promoter for expression instead of an RNA polymerase III promoter

(14). Here the sgRNA is embedded into a larger transcript, which is flanked by self-cleaving ribozyme sequences that will give rise to the mature sgRNA.

Based on this expression system and the *Blastomyces* constructs (12), we have developed a recyclable CRISPR/Cas9 system, which makes use of an inherent feature of *Histoplasma* biology, the maintenance of episomal vectors (5). We embedded expression constructs for both Cas9 nuclease and sgRNA into a larger vector that is flanked by telomeric sequences that facilitate autonomous replication in *Histoplasma* (15). Removal of the selective pressure for the vector leads to the loss of the Cas9/sgRNA plasmid, enabling multiple rounds of CRISPR/Cas9 mediated gene targeting. We have used whole-genome sequencing to further validate that this CRISPR/Cas9 system has limited potential off-target mutations. Finally, we modified the *Blastomyces* system, introducing an endogenous glyceraldehyde-3 phosphate dehydrogenase (*GAPDH*) promoter in place of the *Aspergillus* P_{gpd} regulatory sequence, thereby increasing the efficiency of targeting. Our CRISPR/Cas9 system can be used to introduce gene disruptions in *Histoplasma* at high efficiency with the option to mutate multiple genes.

Results

Assembly of an episomal CRISPR/Cas9 vector system for gene targeting in *Histoplasma*. After several unsuccessful attempts to transform in vitro assembled Cas9/sgRNA RNP complexes into *Histoplasma*, we sought to apply the CRISPR/Cas9 system originally developed by Nødvig et al. to the episomal vector system we utilize for RNAi or gene expression (11). In this case transformed DNA is carried on a linear plasmid with telomeric ends, which facilitates episomal maintenance in *Histoplasma* as

long as selective pressure during growth is maintained. The vector is designed to express both a selective marker gene (either *URA5* or *hph*) and Cas9 from the bidirectional *H2AB* promoter. The sgRNA cassette is essentially the same as developed by Nødvig et al. (11) and includes the well-established *gpdA* promoter and *tef1* terminator sequences from *Aspergillus nidulans*, which drive the expression of the sgRNA precursor as a standard mRNA. The sgRNA itself is composed of a protospacer sequence and tracr RNA that are responsible for binding and activating the Cas9 nuclease as well as guiding the RNP to its destination in the genome. The sgRNA is further flanked by two autocatalytic self-cleaving ribozyme sequences, which will give rise to the mature sgRNA (Fig. 1). After the introduction of a double strand break at the protospacer mediated target site and a potential indel mutation due to error-prone non-homologous end joining repair, one can screen for isolates that have lost the vector when selective pressure is removed from the media.

Potential protospacer sequences for target genes were identified with CRISPOR (http://crispor.tefor.net/) (16). The main criteria for protospacer selection for a specific target gene were a low off-target score as well as a location within the first exon or the first 100 bp of the coding sequence to avoid generating a mutant allele that encodes a partially functional truncated protein due to late frame shift mutations. Protospacer sequences were introduced into the sgRNA cassette via fusion PCR with overlapping primer pairs that contain the 20 bp protospacer sequence as well as a 6bp inverted repeat of the protospacer sequence to ensure correct folding/cleavage of the hammerhead (HH) ribozyme at the 5'-end. For final CRISPR/Cas9 vector assembly, we utilized the Gateway cloning system. We constructed two different Cas9 containing expression vectors with

either *URA5* or *hph* as selection markers, which both incorporated the *ccdB* containing Gateway cassette instead of the sgRNA cassette. Newly assembled sgRNA cassettes were generated in pDONR vectors, which were then recombined with the Cas9 expression vectors. This method allows the generation of a sgRNA cassette that can easily be transferred into either CRISPR/Cas9 vector depending on the selection marker needed.

Highly efficient gene disruption of *RYP2*. We first tried to use this system to disrupt *RYP2*, a key transcriptional regulator required for yeast phase growth at 37°C (Fig. 2A) (17). Successful disruptions of *RYP2* should be identifiable by filamentous colony morphology even under yeast promoting growth conditions. Upon electroporation of the linearized *RYP2* targeting CRISPR/Cas9 vector, 97% of the primary transformants showed at least a partial filamentous phenotype whereas control transformants carrying a Cas9 expressing vector without a sgRNA appeared exclusively in the yeast morphology (Fig. 2B). From the primary transformants we isolated a pure filamentous colony by passaging the primary colony for two generations. Both primary transformants as well as first generation passages appeared as mixed yeast-filamentous colonies, indicating mosaic colonies consisting of wild-type (yeast-form) and *ryp2* mutant (filamentous-form) cells (Fig. 2C). We validated the disruption of the *RYP2* target site in the filamentous mutant by PCR amplification of a 500bp region surrounding the expected cut site followed by Sanger sequencing. We could observe a two-base pair insertion exactly at the protospacer-mediated cut site three bp upstream of the protospacer adjacent motif (PAM) (Fig. 2D). As predicted, sequencing of the same locus from Cas9 expressing control strains without sgRNA all resulted in wild-type sequences.

Successive CRISPR/Cas9 disruption of multiple genes in *Histoplasma*. We investigated whether this system could be used to disrupt multiple genes in *Histoplasma* via vector recycling. We first disrupted *SRE1*, which encodes a repressor of siderophore biosynthesis. Siderophores are small high affinity iron scavengers that serve to transport iron across membranes in bacteria and fungi. When complexed with iron, siderophores confer an orange tinge to colonies, especially when siderophores are in excess as previously observed by targeting *SRE1* with RNAi (18). We reasoned that CRISPR-Cas9-generated *sre1* mutants should be easy to identify on a plate due to increased siderophore formation and thus characteristic orange pigmentation. However, all primary transformants were indistinguishable from the wild-type or Cas9-expressing controls and appeared as creamy white colonies. Similar to primary *ryp2*$^{-}$ mutant transformants, which appeared as mixed colonies of yeast and filamentous phenotype, primary transformants from the *SRE1* targeting CRISPR/Cas9 vector showed a mixed population of cells with either wild-type or the disrupted allele. To identify the frequency of successfully disrupted mutant cells we applied a method commonly used for CRISPR applications in cell lines of higher eukaryotes called Tracking of Indels by Decomposition (TIDE). TIDE identifies the frequency and efficiency of Cas9-mediated frame shift mutations in a mixed pool of CRISPR/Cas9 mediated mutants from Sanger sequencing traces (19). To identify possible frame shift mutations in the *SRE1* target region, we used colony PCR to amplify a 519 bp fragment centered around the putative Cas9 cutting site from colonies of either wild-type, Cas9-expressing controls, or mixed colonies of transformants with the *SRE1*-targeting Cas9 vector. The resulting fragments were sequenced via standard Sanger sequencing and sequence traces were uploaded to the TIDE online platform

(http://tide.nki.nl/). The TIDE algorithm aligns the wild-type sequence with sequence traces of potential mutant/mixed colonies and determines the frequency and alterations in the alignment following the cutting site. The number of aberrant sequences in the mixed pool compared to the wild-type gets interpreted as efficiency of the respective sgRNA to generate mutant cells. Interestingly, our initial colonies of *sre1*$^{-}$ mutants had relatively low disruption efficiency, between 0.5% - 8.6% (Fig. 3A). Passaging the mutants with the highest disruption efficiency successively increased the efficiency of following generations until we obtained a mutant with 96.6% efficiency in generation three, thus approaching homogeneity. The TIDE algorithm further allows the identification of the CRISPR-mediated frame shift mutation, which was an insertion of a guanine at the protospacer mediated cutting site (Fig. 3A, right panel). This insertion was further confirmed via gDNA extraction and sequencing of the respective region (Fig. 3B). The resulting mutant colony was then passaged on non-selective media for three generations and individual colonies were replica-plated on selective and non-selective media to identify mutants that had lost the *SRE1* targeting Cas9 vector. Two individual colonies that carried the guanine insertion mutation and had lost the Cas9 vector were selected for further CRISPR/Cas9 experiments.

As mentioned above, we expected pure *sre1*$^{-}$ mutants to display increased siderophore production, resulting in orange-pigmented colonies especially on high-iron containing media. Phenotypic characterization revealed that the mutants indeed showed increased orange pigmentation compared to wild-type (Fig. 4A). To explore the possibility of making double mutants using CRISPR, we turned to the siderophore biosynthesis pathway. The first enzyme in this pathway, L-ornithine monooxygenase, is

encoded by *SID1*, which is essential for both extra- and intracellular siderophores. Sre1 normally represses *SID1* expression under iron-replete conditions (Fig. 4B) (20, 21). To verify that our CRISPR/Cas9 system can make multiple gene disruptions in the same strain, we disrupted *SID1* in the *sre1*$^-$ mutants followed by Cas9-vector recycling in non-selective media. The resulting *sre1*$^-$ *sid1*$^-$ double mutants were confirmed by Sanger sequencing and compared with wild-type as well as *sre1*$^-$ and *sid1*$^-$ single mutants for their capacity to produce siderophores. The disruption of *SID1* in the *sre1*$^-$ background led to a complete loss of pigmentation (Fig. 4A), consistent with the inability of the mutant to produce siderophores (Fig. 4C).

The selection marker that was originally used to select for the Cas9 vector to generate the *sre1*$^-$ mutant was re-purposed to complement the mutant. We introduced a genomic copy of the *SRE1* wild-type locus as well as an overexpression construct in which the expression of *SRE1* was driven by the constitutive *GAPDH* promoter into the *sre1*$^-$ mutant and analyzed siderophore production levels by chrome azurol S (CAS) assay (Fig. 4C). We observed partial complementation of repression of siderophore biosynthesis when *SRE1* was expressed under its native promoter and complete complementation when it was constitutively expressed under the control of the *GAPDH* promoter. As expected, both *sid1*$^-$ and *sre1*$^-$ *sid1*$^-$ double mutants were unable to produce siderophores (Fig. 4C).

Whole genome sequencing revealed slightly increased SNP accumulations in Cas9 expressing strains. To fully characterize the genotypes of the first round of CRISPR strains, we subjected them to deep sequencing along with several control strains derived from the same frozen WU15 stock as the *sre1*$^-$ CRISPR strains. These isolates included

strains transformed with a Cas9 control vector (Cas9-1 and Cas9-2), a strain passaged without transformation (G217B_ura5_old), and a strain grown in liquid culture for genomic DNA purification without passaging (G217B_ura5_new). The relationships among the sequenced strains are illustrated in Fig. 5.

Based on comparison among strains, we discarded 917 variant positions that could not be distinguished among our sequencing samples, including 314 positions representing clear errors in the reference. This left 36 variant positions, including the targeted CRISPR mutation in *SRE1* (shared by *sre1-1* and *sre1-21*). Strain-unique variant positions, corresponding to mutations acquired after limited passaging, are quite rare: 1 in *sre1-21* and 2 in Cas9-1. An additional 6 variants (2 insertions, 2 adjacent polyG deletions, and 2 point mutations) are shared by sre1-1 and sre1-21. There are 21 variants common to the WU15-derived strains, of which 18 are adjacent to a 3617 bp deletion excising 3 genes including *URA5* (Fig. S1).We attribute both the point mutations and the large deletion to the UV mutagenesis that produced the WU15 strain. Although this strain has been previously reported and is widely used, this is the first precise characterization of the genomic change responsible for the Ura$^-$ phenotype. Finally, there is one short sequence duplication shared by G217B_ura5_new and Cas9-2.

We observed no large deletions in non-repeat regions for Cas9 transformed strains, with or without CRISPR guides.

Cas9 dual sgRNA vectors facilitate complete gene deletions. The method described thus far generates gene disruptions rather than deletions. However, during the course of protocol optimization, we noticed that introducing two sgRNAs into the CRISPR/Cas9 vector that target the same locus resulted in a deletion of the fragment between the

protospacer-mediated cut sites. We decided to explore this phenomenon further by using two sgRNAs with protospacer sequences targeting the start and end of a whole coding region to facilitate complete gene deletions. We designed two sgRNA cassettes that target the 5'- and the 3'- end of the coding sequence for the velvet protein Vea1. *VEA1* RNAi studies have shown that Vea1 is required for appropriate dimorphic switching upon temperature change (22). Primary transformants were screened by PCR using a primer that would anneal to the *VEA1* 5'- and 3'- flanking regions, resulting in two different bands based on the absence or presence of the *VEA1* CDS (Fig. 6A). Selected colonies were passaged and screened by PCR until the *VEA1* wild-type band disappeared. The deletion of the *VEA1* CDS in the mutants was validated by Southern hybridization using probes in either the 5'UTR flanking region of *VEA1* (Fig. 6B) or the *VEA1* CDS (Fig. S2). Phenotypical characterization of the *veal*Δ mutants confirmed the results of Laskowski-Peak et al. (22), which showed a faster rate of filamentation in *VEA1* RNAi strains at room temperature compared to wild-type. Similarly, we observed the appearance of white, filamentous patches much earlier for the *vea1*Δ strains compared to the parental strain (Fig. 6C).

Modulating sgRNA expression alters the frequency of Cas9-mediated editing

To further optimize Cas9-mediated gene editing, we assessed the effect of expressing sgRNAs under the control of a native *Histoplasma* promoter. We constructed episomal Cas9 plasmids driving the expression of an identical mCherry sgRNA under the control of either the *A. nidulans GAPDH* promoter (P_{gpdA}) adapted from Nødvig *et al.* 2015 or the native *Histoplasma* glyceraldehyde 3-phosphate dehydrogenase (*GAPDH*) promoter (P_{GAPDH}) (Fig. 7A). These plasmids were then transformed into a *Histoplasma* strain

(mCherry HcG217B (23)) harboring an integrated mCherry marker driven under the expression of the *CBP1* promoter. The robust mCherry expression in this strain results in yeast colonies that are bright pink by eye with levels of fluorescence that are detectable via microscopy and flow cytometry (Fig. 7B). Following transformation, we initially observed that a majority of P_{GAPDH} transformants were cream colored by eye in contrast to P_{gpdA} transformants that retained some degree of pink color. Following these preliminary observations, two P_{GAPDH} isolates and two P_{gpdA} isolates were selected at random and passaged under selection in liquid culture. These isolates were subsequently used for Sanger sequencing and flow cytometry to quantify editing efficiency and mCherry signal, respectively. Interestingly, our TIDE analysis revealed that in contrast to the average 25% editing efficiency observed in P_{gpdA} transformants, P_{GAPDH} transformants displayed an average editing efficiency of 93% (Fig. 7C). This finding was also corroborated by our flow cytometry data, where 100% of P_{GAPDH}_1 and 94.1% of P_{GAPDH}_2 cells were negative for mCherry signal (Fig. 7D). These findings suggest that optimizing expression of sgRNAs through use of a native promoter can enhance editing efficiency and minimize the passaging time required to generate a pure mutant.

Discussion

Here we describe the development of a recyclable CRISPR/Cas9 system which can be used to introduce gene disruptions or deletions in *Histoplasma*, without leaving major marks in the genome other than the targeted mutations. As proof of principle, we generated disruptions of *RYP2*, *SRE1*, and *SID1*, as well as a complete deletion of *VEA1*. This method allows the rapid generation of targeted mutants with a very low risk for off-target mutations. Furthermore, multiplexing sgRNA expression cassettes in the Cas9

297 expression vector can be used to successfully delete whole genes and has the potential to
298 accelerate gene disruptions for multiple loci.
299 The molecular toolbox for studying the basic biology of *Histoplasma* includes genome
300 wide expression studies, genetic screens based on random insertional mutagenesis, and
301 RNA interference. However, in contrast to other fungi, targeted gene disruptions or
302 replacements are rare, due to the low rate of homologous recombination (24). In the
303 present study we built on technology applied in *Blastomyces* (12) to demonstrate that
304 CRISPR/Cas9 technology can be utilized to generate targeted gene disruptions and
305 deletions in *Histoplasma*. We utilized an inherent feature of *Histoplasma*, the
306 maintenance of extra chromosomal DNA, and embedded both Cas9 and sgRNA
307 expression cassettes into an episomal vector system that can be recycled after successful
308 gene disruption. Initial genome editing efficiency after transformation of the Cas9-
309 sgRNA constructs was not always high in *Histoplasma*, resulting in colonies with mixed
310 populations of wild-type and mutated cells, but successive passaging led to rapid increase
311 in editing efficiency resulting in homogenous mutated colonies after 2-4 passages. This is
312 in contrast to the CRISPR/Cas9 strategy applied in the dimorphic pathogen *Blastomyces*
313 *dermatitidis* where Kujoth et al. could not detect increased genome editing upon
314 successive passaging (12). Interestingly, expressing Cas9-sgRNA constructs under the
315 control of the *Histoplasma GAPDH* promoter rather than the *A. nidulans GAPDH*
316 promoter led to increased efficiency of targeting in *Histoplasma*.
317 We found that the combination of colony PCR and the TIDE algorithm simplifies and
318 streamlines the screening process of primary transformants and passaged isolates to
319 obtain targeted disruptions. It was most helpful to use TIDE as a tool to select

transformants with highest editing efficiency for further passaging to isolate homogeneous mutant colonies. Additionally, we have used TIDE to evaluate general efficiency of different sgRNAs targeting the same genomic locus. This screening is particularly helpful because the efficiency of individual sgRNAs can vary widely for unknown reasons. The G/C content of the protospacer as well as the four bases preceding the PAM sequence seem to have a huge influence on the efficiency of sgRNAs (25, 26). Choosing the most desirable sgRNA can become a compromise between location of the protospacer sequence in the target region and the predicted efficiency of the sgRNA based on its sequence. TIDE can be used after transformation to identify the most efficient sgRNA for a locus with limited protospacer availability.

The delivery of Cas9-sgRNA RNPs into fungal cells is usually achieved either via transformation of *in vitro* assembled RNPs or by integration of expression cassettes for Cas9 and sgRNA into the genome (9, 12, 13, 27, 28). Concerns about potential off-target effects due to irregular Cas9 activity have led to the development of transient Cas9 expression systems, where Cas9 and sgRNA expression cassettes can be removed from the genome after successful gene editing (10, 11, 29). A transient expression system bears several advantages, the first being the ability to reuse selectable marker genes, especially in fungi with limited marker availability. In *Histoplasma*, there are currently three marker genes with documented use: *URA5* (orotate phosphoribosyltransferase), *hph* (hygromycin phosphotranseferase), and *Sh ble* (bleomycin/Zeocin resistance gene). Of these, *URA5* requires the auxotrophic *ura5*$^{-}$ background strain, leaving just two marker genes for genetic manipulations in the wild-type strain. Another advantage of a recyclable transient expression system is the elucidation of complex genetic networks by consecutive gene

343 disruptions or deletions as exemplified here by the successive deletion of *SRE1* and *SID1*.
344 Additionally, loss of the Cas9-sgRNA expression construct allows introduction of a
345 complementation clone without concern that the complementation sequence will be
346 targeted by Cas9. Recycling of the Cas9 nuclease further prevents the risk of potential
347 off-target mutations, which could accumulate due to prolonged Cas9 expression.
348 Interestingly, potential cytotoxic effects due to Cas9 expression in fungi are a matter of
349 debate. Whereas it seems that some fungal groups of the genera *Aspergillus, Candida,*
350 *and Cryptococcus* are not affected by prolonged Cas9 expression, cytotoxic effects have
351 been shown in *Saccharomyces* and *Candida glabrata* (30). However, it is still unclear
352 whether it is the Cas9 expression itself that actually results in increased off-target
353 mutations. We investigated this by comparing the genomes of CRISPR/Cas9 generated
354 mutants to Cas9-only expressing strains and wild-type strains. We observed a slight
355 increase in variants in the genome of the CRISPR-generated mutants compared to wild-
356 type. Five of these variants were strain-unique and 6 were shared among the CRISPR
357 edited mutants. Further experimentation will determine whether these latter 6 mutations
358 will continue to be overrepresented in strains expressing CRISPR/Cas9. Another concern
359 that has been raised for CRISPR-based applications in cells of higher eukaryotes is the
360 potential for large-scale genomic rearrangements in the target region (31). However, we
361 did not observe any large deletions or rearrangements in any of the sequenced isolates.
362 Our results confirm previous observations that CRISPR/Cas9 applications in fungi are
363 generally a robust and suitable alternative to classical molecular biology methods, such as
364 homologous recombination. The approach described here is likely to have a
365 transformative effect on dissecting *Histoplasma* biology.
366

Materials and Methods

***Histoplasma* strains and culture conditions.** All experiments were carried out in the *Histoplasma* G217B *ura5*$^-$ background. A list of generated strains can be found in Table S3. Yeast cultures of *Histoplasma* strains were propagated in liquid Histoplasma macrophage medium (HMM) (32) supplemented with uracil (200 µg/ml), hygromycin (200 µg/ml) or Zeocin (50 µg/ml) as indicated. Liquid cultures were grown at 37°C with 5% CO_2 on an orbital shaker with 120 rpm. For phenotypical characterization of the strains, yeast cultures were diluted to an $OD_{600} = 1$ and 10 µl were spotted on solid HMM plates, which were incubated at 37°C with 5% CO_2.

For cloning purposes either *E. coli* DH5α or One Shot® *ccdB* Survival^{TM} 2 T1^{R} (Invitrogen) for plasmids containing the *ccdB* containing Gateway cassette were used.

Generation of episomal CRISPR/Cas9 vectors. All plasmids and primers used in this study are described in Table S1 and S2. Based on the work of Nødvig et al. (11), we created an episomal vector that expresses fungal codon optimized *cas9* from *Streptococcus pyogenes* as well as a hybrid sgRNA. For the vector backbone we used pBJ209, which was amplified from the RNAi vector pSB23 with primers OAS5744/OAS5745, which introduce ApaI and NheI restriction sites respectively. Next, we amplified the *ccdB* containing Gateway cassette with primers OAS5734/OAS5735 from pSB23, which introduced ClaI restriction sites at 5'- and 3'-ends and cloned the Gateway cassette into the ClaI site of pBJ209, resulting in pBJ213. The codon optimized *cas9* sequence was amplified from pPTS608-Cas9-hyg (12) with primers OAS5736/OAS5737 that introduced NheI- and ApaI-sites at the 5'- and 3'-end as well as attB-sites for subcloning in pDONR. The *cas9* sequence was excised from its larger

amplicon with NheI and ApaI and cloned into NheI/ApaI digested pBJ213 to make pBJ219. Any gRNA cassette cloned into the pDONR vector can be recombined with pBJ219 via Gateway cloning to produce a final CRISPR/Cas9 targeting vector for transformation into *Histoplasma*. Details for individual targeting vectors are given in supplemental material.

Evaluation of protospacer sequences. Protospacer sequences specific for the Sp-Cas9 (20bp-NGG) were designed to target the first exon of the target genes to disrupt the coding sequence as far upstream as possible. Potential candidates were evaluated for specificity and possible off-target sites with the online tool CRISPOR (http://crispor.tefor.net) (16).

TIDE analysis of heterogeneous colonies. To determine the editing efficiency of the respective gRNAs, we used the online tool TIDE (http://tide.nki.nl/) (19). Colonies of positive transformants as well as wild-type controls were subjected to colony PCR to amplify an approximately 500bp fragment of the gRNA mediated target region centered around the putative cutting site. For colony PCR, *Histoplasma* yeast colonies were lysed by boiling in 100 µl 0.02 M NaOH for 10 min. 2 µl of the supernatant was directly used as template for standard PCR reactions with either Phusion or Taq polymerase. The fragments were sequenced by Sanger DNA sequencing. The sequence traces of wild-type and heterogeneous mutated colonies were aligned with the TIDE online tool, which identifies mutations introduced at or near the putative cutting site and determines their approximate frequency in a heterogeneous cell population.

CAS assay for siderophore quantification. The siderophore production level of different mutants was determined using chrome azurol S (CAS) as previously described

(21). *Histoplasma* yeast cultures, grown in triplicate in liquid HMM, were pelleted, washed with PBS and resuspended in RPMI without phenol red to avoid potential interference with the colorimetric assay. The cultures were grown for 24 h at 37°C. The culture supernatant was mixed 1:1 with modified CAS assay solution (0.6 M HDTMA, 15 µM $FeCl_3$, 150 µM CAS, 0.5 M MES, 3.4 mM 5-sulfosalicyclic acid) (33) in a 96 well plate and incubated for 3-4 h. OD_{630} was measured with a plate reader and normalized to OD_{600} of the cultures to account for cell density.

Whole genome library preparation and sequencing. Dual-indexed paired-end libraries for whole genome sequencing were prepared with the Nextera DNA Flex Library Prep Kit from Illumina. Individual libraries were barcoded with Nextera DNA CD Indexes (Illumina) and analyzed for average size distribution and concentration on a High Sensitivity DNA Bioanalyzer chip from Agilent Technologies. Fragments of individual libraries had an average size distribution of 500-550 bp and 5 ng of each library were pooled for multiplexed sequencing. All 6 strains were sequenced in a single lane on an Illumina HiSeq 4000 at the UCSF Center for Advanced Technology (UCSF CAT) yielding 101-mer paired-end reads with ~400x coverage of the genome per strain. To distinguish mutations in the WU15 parental strain from errors in the reference, we additionally analyzed reads from wild-type G217B (34) with ~200x coverage of the genome.

NGS data analysis. The raw data are available at the NCBI Sequence Read Archive (SRA) under SRA accession PRJNA971667. The reads were analyzed as illustrated in Supplemental Fig. S3. In summary, reads were aligned to the 11/30/2004 version of the G217B genome assembly from the Genome Sequencing Center (GSC) at Washington

University as mirrored at https://histo.ucsf.edu/downloads/ using BWA-MEM (35) with GATK (36) indel realignment. Long repeat sequences were annotated in the reference genome using LTRHARVEST (37) and REPEATMASKER (A.F.A. Smit, R. Hubley & P. Green RepeatMasker at http://repeatmasker.org) queried with repeat families identified by the GSC as well as a representative full length MAGGY LTR retro transposon. Large deletions were identified as regions of at least 300 bp with fewer than 10 reads per base pair interrupted by higher coverage regions of less than 50 bp. Deletions overlapping repeat annotations were removed, and the remaining per-strain deletions were normalized by clustering on genome location to generate a consistent set of deletion coordinates across strains. To identify short sequence variations, the full set of aligned reads was run through SAMTOOLS MPILEUP (http://www.htslib.org/doc/samtools-mpileup.html) and BCFTOOLS CALL (http://www.htslib.org/doc/bcftools.html). A variant allele was assigned to a strain if it was supported by at least 85% of the reads at the variant site for sites with at least 10 aligned reads for the given strain; variant sites where no allele passed these support criteria were flagged as ambiguous. Variant sites with zero or one alleles unambiguously assigned across all strains (*e.g.*, errors in the reference sequence) were removed as were sites overlapping annotated repeat regions or large deletions. Large deletions and variant sites were then classified among strains as summarized in Fig. 5.

Southern hybridization of *vea1*Δ mutants. A 1052-bp probe to the 5' UTR of *VEA1* was amplified from G217B *ura5*$^{-}$ genomic DNA using primer set OAS6659/OAS6660. A second 1013-bp probe to the *VEA1* CDS was amplified from G217B ura5^{-} genomic DNA using primer set OAS6663/OAS1969. In separate reactions the resulting PCR fragments

459 were coupled with an alkaline phosphatase enzyme using the Amersham Gene Images
460 AlkPhos Direct Labelling and Detection System (GE Healthcare), according to the
461 manufacturers protocol. Genomic DNA from the parental strain G217B *ura5*$^{-}$ and the
462 mutant strains was isolated by phenol chloroform extraction. In duplicate, 15 µg of
463 genomic DNA from both samples was digested with restriction enzyme *Bgl*II for 1 hour
464 at 37˚C. Digested DNA was size separated by gel electrophoresis on a 0.7 % agarose gel
465 and transferred to a Hybond-N+ nylon membrane (Amersham Biosciences). Membrane
466 bound digested genomic DNA was hybridized at 60˚C overnight with either the probe to
467 the 5' UTR or to the *VEA1* CDS. Finally, the membranes were visualized by using CDP-
468 Star Chemiflourescent detection system (GE Healthcare).
469 **Flow cytometry.** Transformants were selected at random and grown in liquid HMM with
470 plasmid selection. Cultures were passaged 24 hours prior to harvest to obtain mid-log
471 phase cells with an OD_{600} between 5-7. Approximately 1.25 E7 cells per sample were
472 sonicated, washed, and spun down with D-PBS before being fixed on ice with BD
473 Stabilizing Fixative (BD Biosciences). Once fixed, samples were washed and
474 resuspended in D-PBS and analyzed using a BD LSRII Flow Cytometer in the UCSF
475 Parnassus Flow Core. mCherry fluorescence signal in each sample was analyzed and
476 quantified using FlowJo v. 10. mCherry positive and negative control strains were used to
477 set gates for quantifying signal across all transformants.
478

479 **References**

480 1. Sil A, Andrianopoulos A. 2014. Thermally Dimorphic Human Fungal Pathogens
481 – Polyphyletic Pathogens with a Convergent Pathogenicity Trait. Cold Spring
482 Harbor perspectives in medicine 5:a019794.

2. Manos NE, Ferebee SH, Kerschbaum WF. 1956. Geographic variation in the prevalence of histoplasmin sensitivity. Dis Chest 29:649-68.
3. Armstrong PA, Jackson BR, Haselow D, Fields V, Ireland M, Austin C, Signs K, Fialkowski V, Patel R, Ellis P, Iwen PC, Pedati C, Gibbons-Burgener S, Anderson J, Dobbs T, Davidson S, McIntyre M, Warren K, Midla J, Luong N, Benedict K. 2018. Multistate Epidemiology of Histoplasmosis, United States, 2011-2014. Emerging infectious diseases 24:425-431.
4. Boyce KJ, Andrianopoulos A. 2015. Fungal dimorphism: the switch from hyphae to yeast is a specialized morphogenetic adaptation allowing colonization of a host. FEMS Microbiology Reviews 39:797-811.
5. Woods JP, Heinecke EL, Goldman WE. 1998. Electrotransformation and expression of bacterial genes encoding hygromycin phosphotransferase and beta-galactosidase in the pathogenic fungus Histoplasma capsulatum. Infection and Immunity 66:1697-1707.
6. DiCarlo JE, Norville JE, Mali P, Rios X, Aach J, Church GM. 2013. Genome engineering in Saccharomyces cerevisiae using CRISPR-Cas systems. Nucleic Acids Research 41:4336-4343.
7. Liu Q, Shi X, Song L, Liu H, Zhou X, Wang Q, Zhang Y, Cai M. 2019. CRISPR-Cas9-mediated genomic multiloci integration in Pichia pastoris. Microbial cell factories 18:144.
8. Liu R, Chen L, Jiang Y, Zhou Z, Zou G. 2015. Efficient genome editing in filamentous fungus Trichoderma reesei using the CRISPR/Cas9 system. Cell discovery 1:15007-11.
9. Matsu-ura T, Baek M, Kwon J, Hong C. 2015. Efficient gene editing in Neurospora crassa with CRISPR technology. Fungal biology and biotechnology 2:4.
10. Nguyen N, Quail MMF, Hernday AD. 2017. An Efficient, Rapid, and Recyclable System for CRISPR-Mediated Genome Editing in Candida albicans. mSphere 2.
11. Nødvig CS, Nielsen JB, Kogle ME, Mortensen UH. 2015. A CRISPR-Cas9 System for Genetic Engineering of Filamentous Fungi. PLoS ONE 10:e0133085.
12. Kujoth GC, Sullivan TD, Merkhofer R, Lee T-J, Wang H, Brandhorst T, Wüthrich M, Klein BS. 2018. CRISPR/Cas9-Mediated Gene Disruption Reveals the Importance of Zinc Metabolism for Fitness of the Dimorphic Fungal Pathogen Blastomyces dermatitidis. mBio 9:e00412-18.
13. Al Abdallah Q, Ge W, Fortwendel JR. 2017. A Simple and Universal System for Gene Manipulation in Aspergillus fumigatus: In Vitro-Assembled Cas9-Guide RNA Ribonucleoproteins Coupled with Microhomology Repair Templates. mSphere 2.
14. Nødvig CS, Hoof JB, Kogle ME, Jarczynska ZD, Lehmbeck J, Klitgaard DK, Mortensen UH. 2018. Efficient oligo nucleotide mediated CRISPR-Cas9 gene editing in Aspergilli. Fungal Genetics and Biology 115:78-89.
15. Woods JP, Goldman WE. 1993. Autonomous Replication of Foreign DNA in Histoplasma capsulatum: Role of Native Telomeric Sequences. Journal of Bacteriology 175:636-641.
16. Haeussler M, Schönig K, Eckert H, Eschstruth A, Mianné J, Renaud J-B, Schneider-Maunoury S, Shkumatava A, Teboul L, Kent J, Joly J-S, Concordet J-

P. 2016. Evaluation of off-target and on-target scoring algorithms and integration into the guide RNA selection tool CRISPOR. Genome Biology 17:148.

17. Webster RH, Sil A. 2008. Conserved factors Ryp2 and Ryp3 control cell morphology and infectious spore formation in the fungal pathogen Histoplasma capsulatum. Proceedings of the National Academy of Sciences of the United States of America 105:14573-14578.

18. Hwang LH, Seth E, Gilmore SA, Sil A. 2012. SRE1 regulates iron-dependent and -independent pathways in the fungal pathogen Histoplasma capsulatum. Eukaryotic Cell 11:16-25.

19. Brinkman EK, Chen T, Amendola M, van Steensel B. 2014. Easy quantitative assessment of genome editing by sequence trace decomposition. Nucleic Acids Research 42:e168.

20. Eisendle M, Oberegger H, Zadra I, Haas H. 2003. The siderophore system is essential for viability of Aspergillus nidulans: functional analysis of two genes encoding l-ornithine N 5-monooxygenase (sidA) and a non-ribosomal peptide synthetase (sidC). Molecular Microbiology 49:359-375.

21. Hwang LH, Mayfield JA, Rine J, Sil A. 2008. Histoplasma Requires SID1, a Member of an Iron-Regulated Siderophore Gene Cluster, for Host Colonization. PLoS Pathogens 4:e1000044.

22. Laskowski-Peak MC, Calvo AM, Rohrssen J, Smulian AG. 2012. VEA1 is required for cleistothecial formation and virulence in Histoplasma capsulatum. Fungal Genetics and Biology 49:838-846.

23. Van Prooyen N, Henderson CA, Hocking Murray D, Sil A. 2016. CD103+ Conventional Dendritic Cells Are Critical for TLR7/9-Dependent Host Defense against Histoplasma capsulatum, an Endemic Fungal Pathogen of Humans. PLoS Pathogens 12:e1005749.

24. Woods JP, Retallack DM, Heinecke EL, Goldman WE. 1998. Rare Homologous Gene Targeting in Histoplasma capsulatum: Disruption of the URA5Hc Gene by Allelic Replacement. Journal of Bacteriology 180:5135-5143.

25. Graf R, Li X, Chu VT, Rajewsky K. 2019. sgRNA Sequence Motifs Blocking Efficient CRISPR/Cas9-Mediated Gene Editing. Cell Reports 26:1098-1103.e3.

26. Xu H, Xiao T, Chen C-H, Li W, Meyer CA, Wu Q, Wu D, Cong L, Zhang F, Liu JS, Brown M, Liu XS. 2015. Sequence determinants of improved CRISPR sgRNA design. Genome Research 25:1147-1157.

27. Arras SDM, Chua SMH, Wizrah MSI, Faint JA, Yap AS, Fraser JA. 2016. Targeted Genome Editing via CRISPR in the Pathogen Cryptococcus neoformans. PLoS ONE 11:e0164322.

28. Fuller KK, Chen S, Loros JJ, Dunlap JC. 2015. Development of the CRISPR/Cas9 System for Targeted Gene Disruption in Aspergillus fumigatus. Eukaryotic Cell 14:1073-1080.

29. Tran VG, Cao M, Fatma Z, Song X, Zhao H. 2019. Development of a CRISPR/Cas9-Based Tool for Gene Deletion in Issatchenkia orientalis. mSphere 4.

30. Mitchell AP. 2017. Location, location, location: Use of CRISPR-Cas9 for genome editing in human pathogenic fungi. PLoS Pathogens 13:e1006209.

574 31. Kosicki M, Tomberg K, Bradley A. 2018. Repair of double-strand breaks induced
575 by CRISPR-Cas9 leads to large deletions and complex rearrangements. Nature
576 Biotechnology 36:765-771.
577 32. Worsham PL, Goldman WE. 1988. Quantitative plating of Histoplasma
578 capsulatum without addition of conditioned medium or siderophores. Journal of
579 medical and veterinary mycology : bi-monthly publication of the International
580 Society for Human and Animal Mycology 26:137-143.
581 33. Alexander DB, Zuberer DA. 1991. Use of chrome azurol S reagents to evaluate
582 siderophore production by rhizosphere bacteria. Biology and Fertility of Soils
583 doi:10.1128/JB.183.10.3117-3126.2001:39-45.
584 34. Sepúlveda VE, Márquez R, Turissini DA, Goldman WE, Matute DR. 2017.
585 Genome Sequences Reveal Cryptic Speciation in the Human Pathogen
586 Histoplasma capsulatum. mBio 8.
587 35. Li H. 2013. Aligning sequence reads, clone sequences and assembly contigs with
588 BWA-MEM. arxivorg:1-3.
589 36. McKenna A, Hanna M, Banks E, Sivachenko A, Cibulskis K, Kernytsky A,
590 Garimella K, Altshuler D, Gabriel S, Daly M, DePristo MA. 2010. The Genome
591 Analysis Toolkit: a MapReduce framework for analyzing next-generation DNA
592 sequencing data. Genome Research 20:1297-1303.
593 37. Valencia JD, Girgis HZ. 2019. LtrDetector: A tool-suite for detecting long
594 terminal repeat retrotransposons de-novo. BMC Genomics 20:450.
595

596

597 **Figure Legends**

598 **Figure 1. Schematic representation of the CRISPR/Cas9 mediated targeted gene**

599 **disruption in *H. capsulatum*.** Under selective pressure the CRISPR/Cas9 plasmid is

600 maintained in *Histoplasma* as an extrachromosomal vector, which carries both a codon

601 optimized version of Cas9 and the sgRNA (based on the concept of Nødvig et al., 2015).

602 The sgRNA is expressed as a precursor driven by a constitutive RNA polymerase II

603 promoter ($gpdA^{P}$), resulting in a larger mRNA-like transcript with 5'-cap and poly-(A)

604 tail. The mature sgRNA gets excised from its larger transcript via the action of two

605 flanking ribozyme sequences (hammerhead, HH and hepatitis delta virus, HDV). The

606 sgRNA then recruits the Cas9 nuclease to a protospacer (PS)-mediated target site in the

607 genome, where it cuts the gDNA. The resulting double-strand break is repaired by the

608 non-homologous end joining (NHEJ) mechanism, an error-prone process that often
609 introduces small indel mutations. Growing the resultant mutant strain under non-selective
610 conditions (*i.e.* in the presence of uracil) allows loss of the CRISPR/Cas9 vector, which
611 then permits re-use of the *URA5* marker for subsequent transformations.

612 **Figure 2. CRISPR/Cas9 mediated disruption of *RYP2*.** (A) Schematic representation
613 of *RYP2*-mediated regulation of the dimorphic switch in *H. capsulatum*. At mammalian
614 body temperature, Ryp2 is required to promote yeast-phase growth. (B) Primary
615 transformants carrying the CRISPR/Cas9 vector targeting *RYP2*. Whereas transformants
616 carrying a Cas9-only expressing control vector exhibited a smooth yeast-colony shape,
617 transformants carrying the *RYP2* targeting CRISPR/Cas9 vector showed predominantly a
618 wrinkled/filamentous phenotype. (C) Phenotypes of first-generation and second-
619 generation *ryp2*$^{-}$ mutants displaying the gradual increase from a mixed yeast/filamentous
620 colony shape to a completely filamentous phenotype. Colonies also showed increased red
621 pigmentation indicating altered secondary metabolism associated with filamentous
622 growth. (D) Sanger sequencing of the *RYP2* target region of the WT and the second-
623 generation *ryp2*$^{-}$ mutant revealed an insertion of TG in the protospacer-mediated target
624 region in the mutant causing a frame-shift mutation in the first exon.

625 **Figure 3. Evaluation of *sre1*$^{-}$ disruption mutants with the online platform TIDE.**
626 Transformants with a *SRE1*-targeting CRISPR/Cas9 vector either directly after
627 transformation or after each passaging were analyzed with TIDE
628 (https://tide.deskgen.com), which detects the predominant mutations (i.e. deletions or
629 insertions) as well as their frequencies. To do so, approximately 500 bp of the sgRNA
630 mediated target sequence were amplified via colony PCR from a control strain as well as

631 mutant colonies harboring the mutation of interest. The DNA fragments were sequenced
632 by standard Sanger sequencing and compared with the TIDE platform. This online tool
633 aligns the first part of the sequences before the anticipated cutting site and calculates the
634 frequency of aberrant sequences following the cutting site for the mutant colony, in this
635 case a disruption mutant of *SRE1* (96.6%) compared to the control sequence. The bottom
636 of panel A shows the gene-editing efficiency of the mutant isolates after subsequent
637 generations of passaging based on TIDE analysis. The gene editing efficiency increases
638 for most colonies after each passaging, resulting in homogeneous mutant isolates after
639 three passages. An additional passage on non-selective medium (*i.e.* in the presence of
640 uracil) resulted in the loss of the vector. (B) Sequencing of the final mutants after Cas9
641 vector loss confirmed a G insertion in the first exon of the *sre1*$^{-}$ mutants resulting in a
642 premature stop codon after 144 bp.

643 **Figure 4. CRISPR/Cas9 vector recycling allows successive gene disruptions and**
644 **complementation.** (A) CRISPR/Cas9 vector recycling in the *sre1*$^{-}$ mutants allowed re-
645 use of the *URA5* marker to target a second gene in the *sre1*$^{-}$ background. The loss of
646 *SRE1* resulted in derepressed siderophore expression, which led to orange pigmentation
647 of the colonies due to increased iron-bound siderophores, especially on high iron
648 containing media. Disruption of *SID1* in the *sre1*$^{-}$ background, which encodes the first
649 enzyme in the siderophore biosynthesis pathway (as diagrammed in B) resulted in
650 complete abolishment of siderophore production, indicated by the loss of orange
651 pigmentation of the colonies of the *sre1*$^{-}$ *sid1*$^{-}$ double mutants. (C) After loss of the Cas9
652 plasmid in the *sre1*$^{-}$ mutant, the *URA5* marker gene was available for selection of
653 complementation plasmids. Siderophore production was analyzed with the CAS assay

and showed partial complementation when *SRE1* was expressed under its native promoter and almost complete complementation when *SRE1* was overexpressed under the control of the constitutive *GAPDH* promoter (OE). In contrast, both *sid1*$^{-}$ and *sre1*$^{-}$ *sid1*$^{-}$ double mutants showed no siderophore production as expected.

Figure 5. Validation of the CRISPR/Cas9 system via whole genome sequencing. We compared the genomes of two CRISPR/Cas9 generated mutants (*sre1-1*, *sre1-21*) with Cas9 only expressing control strains (*Cas9-1*, *Cas9-2*) and the parental strain from which we extracted gDNA for deep sequencing either before (G217B_ura5_old) or after passaging along with the CRISPR mutants (G217B_ura5_new). The diagram shows the strain lineages and whether strains were transformed and passaged for gene-disruption or control. Strain unique variant are given in red parenthesis including the targeted CRISPR/Cas9 mutation.

Figure 6. sgRNA multiplexing for complete gene deletions. We introduced two sgRNA cassettes into the Cas9 expressing vector, targeting the 5'- and 3'-end of the *VEA1* CDS respectively. Colony PCR of primary transformants (lower part of panel A) resulted in two bands for 4 of 10 isolates and only one band for two isolates, indicating partial or complete loss of the *VEA1* CDS in those mutants. WT indicates wild-type. (B) Southern hybridization of *vea1*Δ mutants confirmed the deletion of the *VEA1* CDS in two independent mutants. Location of the probe is shown in the upper part of panel B and the Southern blot is shown in the lower part of panel B. WT indicates wild-type. (C) Phenotypical characterization of the mutants grown at room temperature (RT) was performed by spotting dilutions of wild-type (G217B *ura5*$^{-}$) and *vea1*Δ mutant strains on plates. The *vea1*Δ mutants displayed accelerated filamentation as compared to the

677 parental strain as indicated by the increased density of fluffy white filamentous growth.
678 The difference between wild-type and mutant strains was most pronounced after six days
679 of incubation.

680 **Figure 7. Cas9-sgRNAs expressed under the control of the *Histoplasma* GAPDH**
681 **promoter showed increased editing efficiency.** A) Schematic displaying experimental
682 approach. Plasmids containing either the *A. nidulans* GAPDH promoter adapted from
683 Nødvig et al. 2015 (P_{gpdA}) or the native *Histoplasma* GAPDH promoter (P_{GAPDH}) driving
684 the expression of an identical mCherry targeting guide RNA were transformed into the
685 mCherryHcG217B strain and used to assess differences in editing efficiencies. B) Plate
686 images of the parental mCherryHcG217B strain alongside transformants selected from
687 each plasmid transformation that were subsequently used for Sanger sequencing and flow
688 cytometry. C) Indel spectrum of two individual isolates obtained from each plasmid
689 transformation. Sanger sequencing of the mCherry locus was used to conduct TIDE
690 analysis (https://tide.nki.nl/) to quantify the frequency of insertions and deletions
691 following the predicted cut site. D) Histograms displaying measurements of mCherry
692 signal acquired through flow cytometry. Overlay plots display normalized counts for each
693 isolate in comparison to the starting mCherryHcG217B strain. E) Quantification of flow
694 data displaying percentage of mCherry+ cells within each isolate.
695

696 **Acknowledgements**

697 We thank Gregory Kujoth and Bruce Klein for sharing critical CRISPR reagents. We
698 thank the UCSF Parnassus Flow CoLab RRID:SCR_018206 and DRC Center Grant NIH
699 P30 DK063720 for flow cytometry instruments and support.

700 This work was supported by NIAID grant 2R37AI066224 to AS as well as funds from
701 Chan Zuckerberg Biohub – San Francisco to AS. AS is a Chan Zuckerberg Biohub – San
702 Francisco Investigator. The funders had no role in study design, data collection and
703 interpretation, or the decision to submit the work for publication.

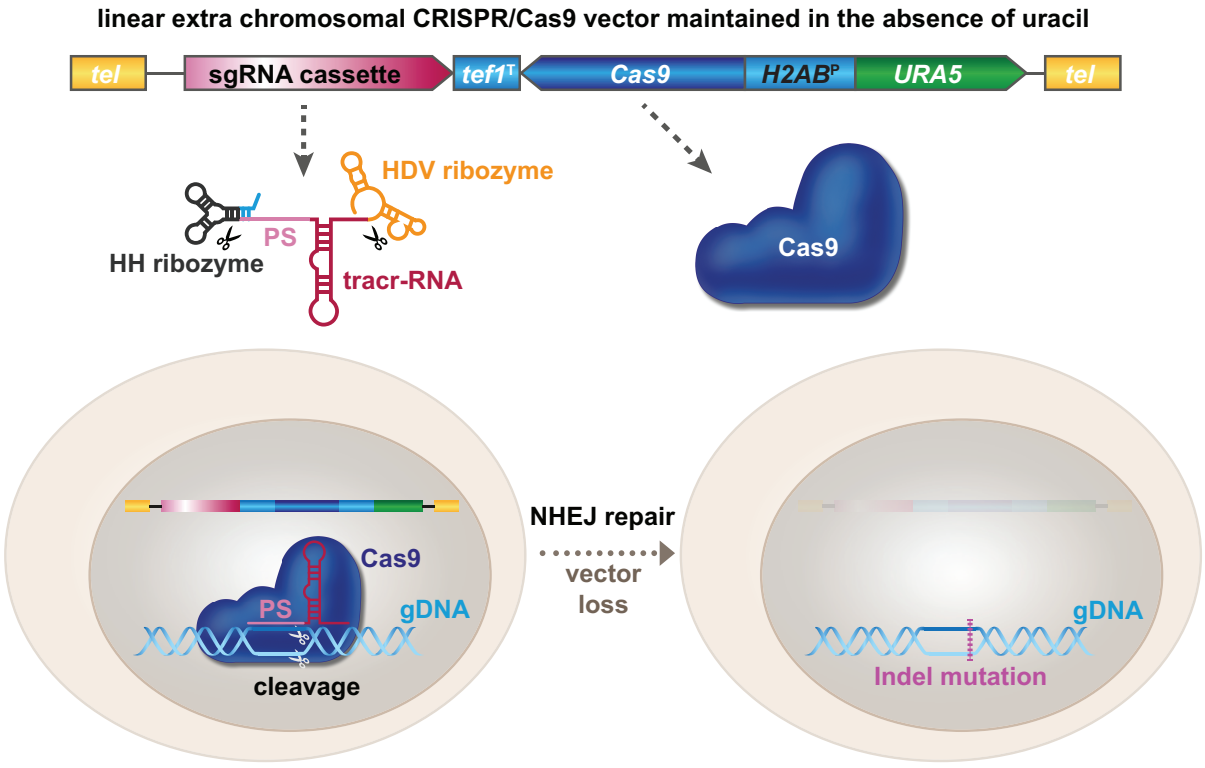

Figure 1. Schematic representation of the CRISPR/Cas9 mediated targeted gene disruption in *H. capsulatum*. Under selective pressure the CRISPR/Cas9 plasmid is maintained in *Histoplasma* as an extrachromosomal vector, which carries both a codon optimized version of Cas9 and the sgRNA (based on the concept of Nødvig et al., 2015). The sgRNA is expressed as a precursor driven by a constitutive RNA polymerase II promoter (*gpdA*^{P}), resulting in a larger mRNA-like transcript with 5'-cap and poly-(A) tail. The mature sgRNA gets excised from its larger transcript via the action of two flanking ribozyme sequences (hammerhead, HH and hepatitis delta virus, HDV). The sgRNA then recruits the Cas9 nuclease to a protospacer (PS)-mediated target site in the genome, where it cuts the gDNA. The resulting double-strand break is repaired by the non-homologous end joining (NHEJ) mechanism, an error-prone process that often introduces small indel mutations. Growing the resultant mutant strain under non-selective conditions (*i.e.* in the presence of uracil) allows loss of the CRISPR/Cas9 vector, which then permits re-use of the *URA5* marker for subsequent transformations.

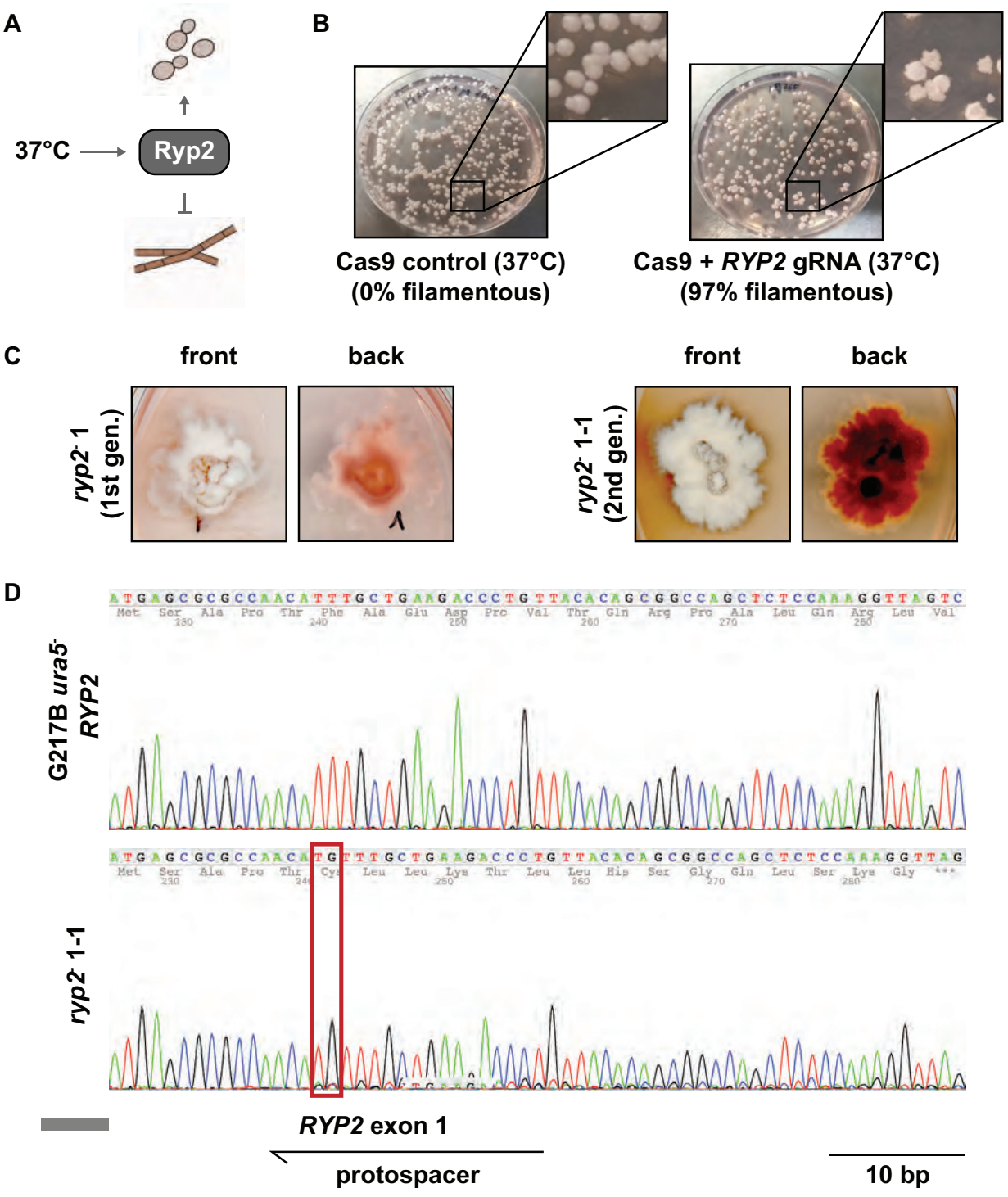

Figure 2. CRISPR/Cas9 mediated disruption of *RYP2*. (A) Schematic representation of *RYP2*-mediated regulation of the dimorphic switch in *H. capsulatum*. At mammalian body temperature, Ryp2 is required to promote yeast-phase growth. (B) Primary transformants carrying the CRISPR/Cas9 vector targeting *RYP2*. Whereas transformants carrying a Cas9-only expressing control vector exhibited a smooth yeast-colony shape, transformants carrying the *RYP2* targeting

CRISPR/Cas9 vector showed predominantly a wrinkled/filamentous phenotype. (C) Phenotypes of first-generation and second-generation *ryp2*$^{-}$ mutants displaying the gradual increase from a mixed yeast/filamentous colony shape to a completely filamentous phenotype. Colonies also showed increased red pigmentation indicating altered secondary metabolism associated with filamentous growth. (D) Sanger sequencing of the *RYP2* target region of the WT and the second-generation *ryp2*$^{-}$ mutant revealed an insertion of TG in the protospacer-mediated target region in the mutant causing a frame-shift mutation in the first exon.

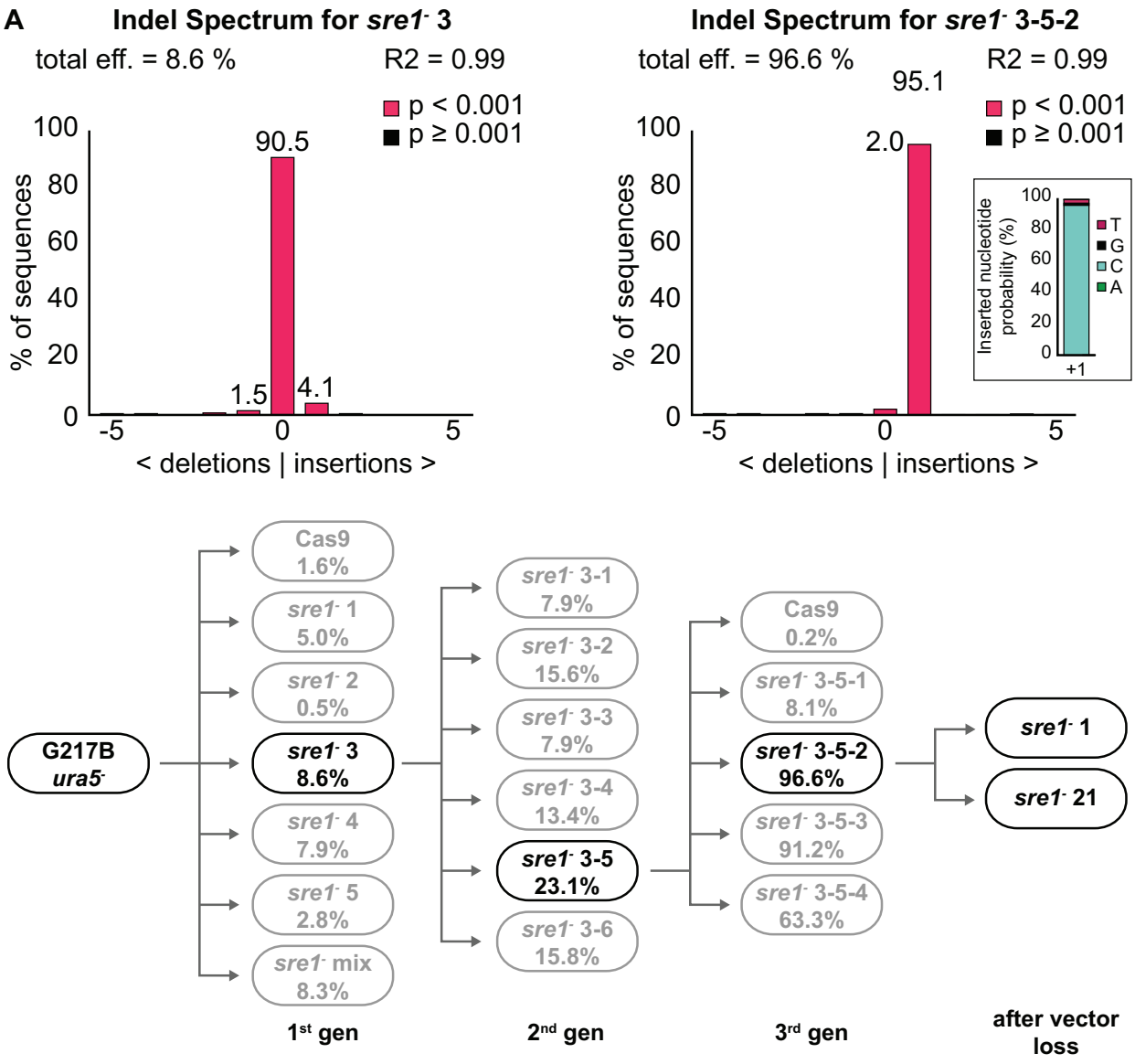

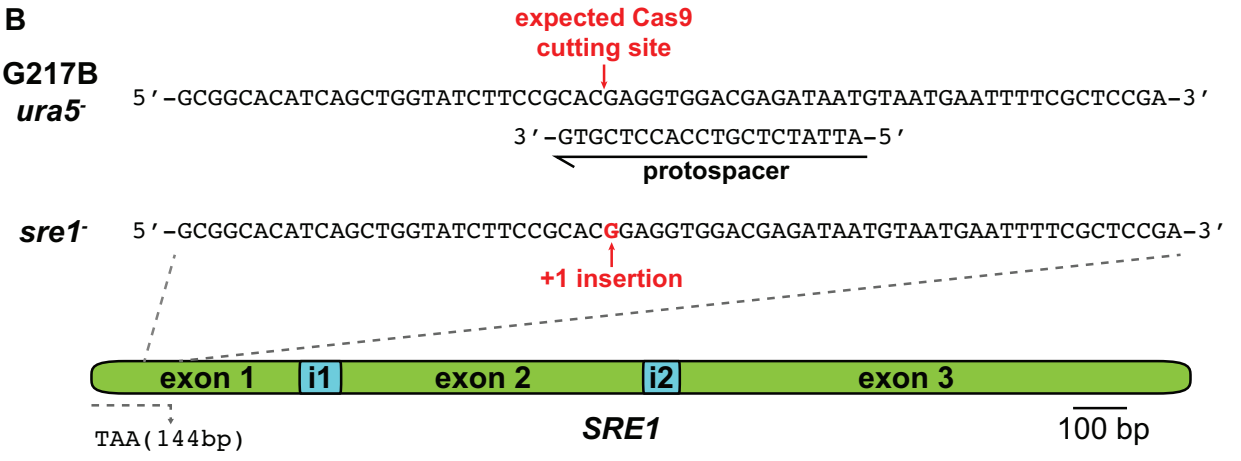

Figure 3. Evaluation of *sre1*$^{-}$ disruption mutants with the online platform TIDE. Transformants with a *SRE1*-targeting CRISPR/Cas9 vector either directly after transformation or after each passaging were analyzed with TIDE (https://tide.deskgen.com), which detects the predominant mutations (i.e. deletions or insertions) as well as their frequencies. To do so, approximately 500 bp of the sgRNA mediated target sequence were amplified via colony PCR from a control strain as well as mutant colonies harboring the mutation of interest. The DNA fragments were sequenced by standard Sanger sequencing and compared with the TIDE platform. This online tool aligns the first part of the sequences before the anticipated cutting site and calculates the frequency of aberrant sequences following the cutting site for the mutant colony, in this case a disruption mutant of *SRE1* (96.6%) compared to the control sequence. The bottom of panel A shows the gene-editing efficiency of the mutant isolates after subsequent generations of passaging based on TIDE analysis. The gene editing efficiency increases for most colonies after each passaging, resulting in homogeneous mutant isolates after three passages. An additional passage on non-selective medium (*i.e.* in the presence of uracil) resulted in the loss of the vector. (B) Sequencing of the final mutants after Cas9 vector loss confirmed a G insertion in the first exon of the *sre1*$^{-}$ mutants resulting in a premature stop codon after 144 bp.

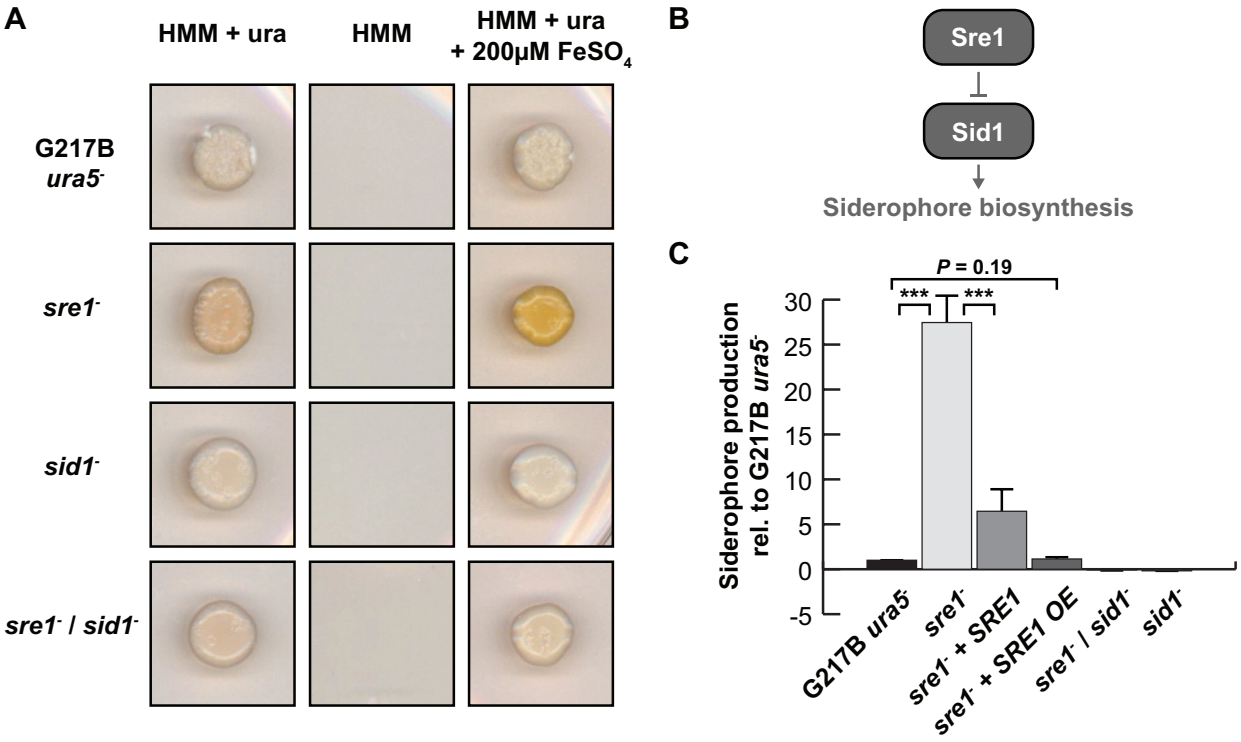

Figure 4. CRISPR/Cas9 vector recycling allows successive gene disruptions and complementation. (A) CRISPR/Cas9 vector recycling in the *sre1*$^{-}$ mutants allowed re-use of the *URA5* marker to target a second gene in the *sre1*$^{-}$ background. The loss of *SRE1* resulted in derepressed siderophore expression, which led to orange pigmentation of the colonies due to increased iron-bound siderophores, especially on high iron containing media. Disruption of *SID1* in the *sre1*$^{-}$ background, which encodes the first enzyme in the siderophore biosynthesis pathway (as diagrammed in B) resulted in complete abolishment of siderophore production, indicated by the loss of orange pigmentation of the colonies of the *sre1*$^{-}$ *sid1*$^{-}$ double mutants. (C) After loss of the Cas9 plasmid in the *sre1*$^{-}$ mutant, the *URA5* marker gene was available for selection of complementation plasmids. Siderophore production was analyzed with the CAS assay and showed partial complementation when *SRE1* was expressed under its native promoter and almost complete complementation when *SRE1* was overexpressed under the control of the constitutive *GAPDH* promoter (OE). In contrast, both *sid1*$^{-}$ and *sre1*$^{-}$ *sid1*$^{-}$ double mutants showed no siderophore production as expected.

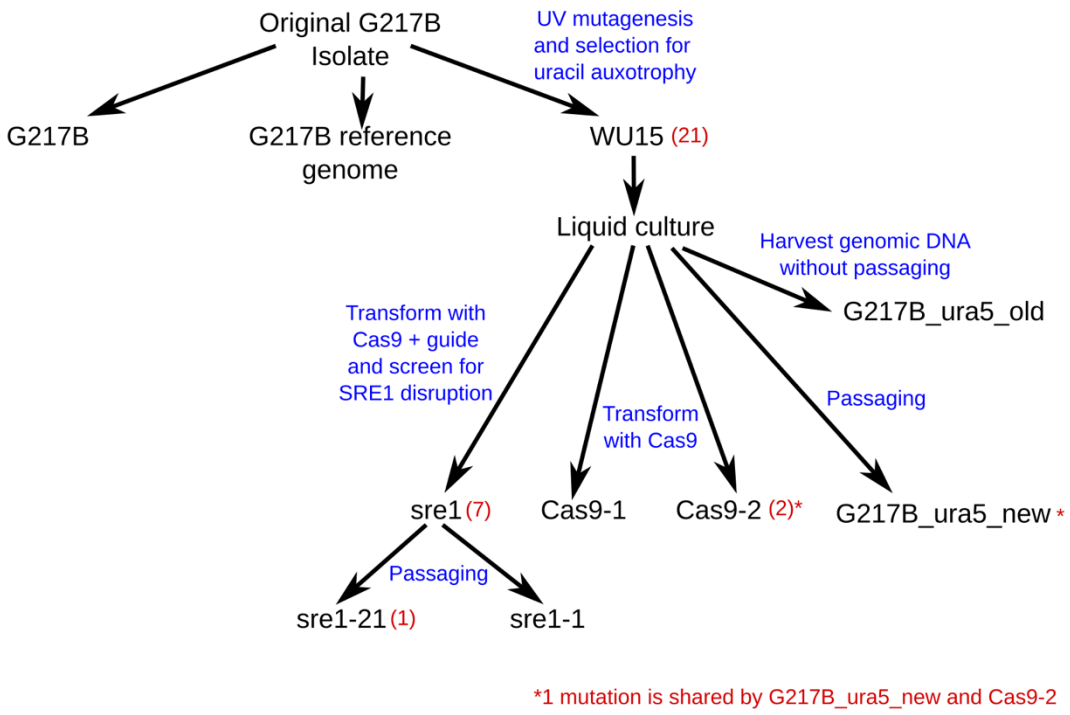

Figure 5. Validation of the CRISPR/Cas9 system via whole genome sequencing.
We compared the genomes of two CRISPR/Cas9 generated mutants (*sre1-1*, *sre1-21*) with Cas9 only expressing control strains (*Cas9-1*, *Cas9-2*) and the parental strain from which we extracted gDNA for deep sequencing either before (G217B_ura5_old) or after passaging along with the CRISPR mutants (G217B_ura5_new). The diagram shows the strain lineages and whether strains were transformed and passaged for gene-disruption or control. Strain unique variant are given in red parenthesis including the targeted CRISPR/Cas9 mutation.

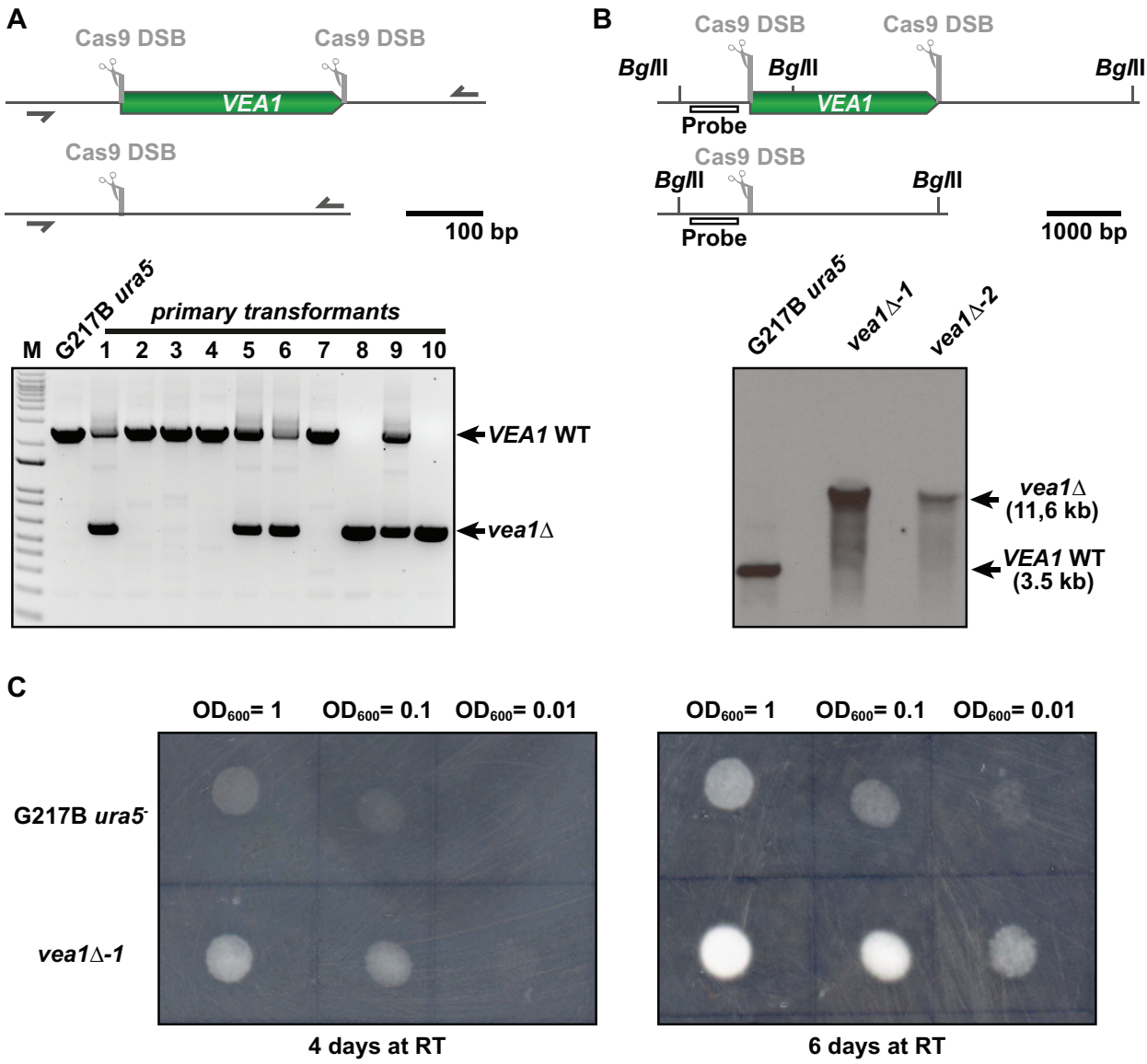

Figure 6. sgRNA multiplexing for complete gene deletions. We introduced two sgRNA cassettes into the Cas9 expressing vector, targeting the 5'- and 3'-end of the *VEA1* CDS respectively. Colony PCR of primary transformants (lower part of panel A) resulted in two bands for 4 of 10 isolates and only one band for two isolates, indicating partial or complete loss of the *VEA1* CDS in those mutants. WT indicates wild-type. (B) Southern hybridization of *vea1*Δ mutants confirmed the deletion of the *VEA1* CDS in two independent mutants. Location of the probe is shown in the upper part of panel B and the Southern blot is shown in the lower part of panel B. WT indicates wild-type. (C) Phenotypical characterization of the mutants grown at room temperature (RT) was performed by spotting dilutions of wild-type (G217B *ura5*$^-$) and *vea1*Δ mutant strains on plates. The *vea1*Δ mutants displayed accelerated filamentation as compared to the parental strain as indicated by the increased density of fluffy white filamentous

growth. The difference between wild-type and mutant strains was most pronounced after six days of incubation.

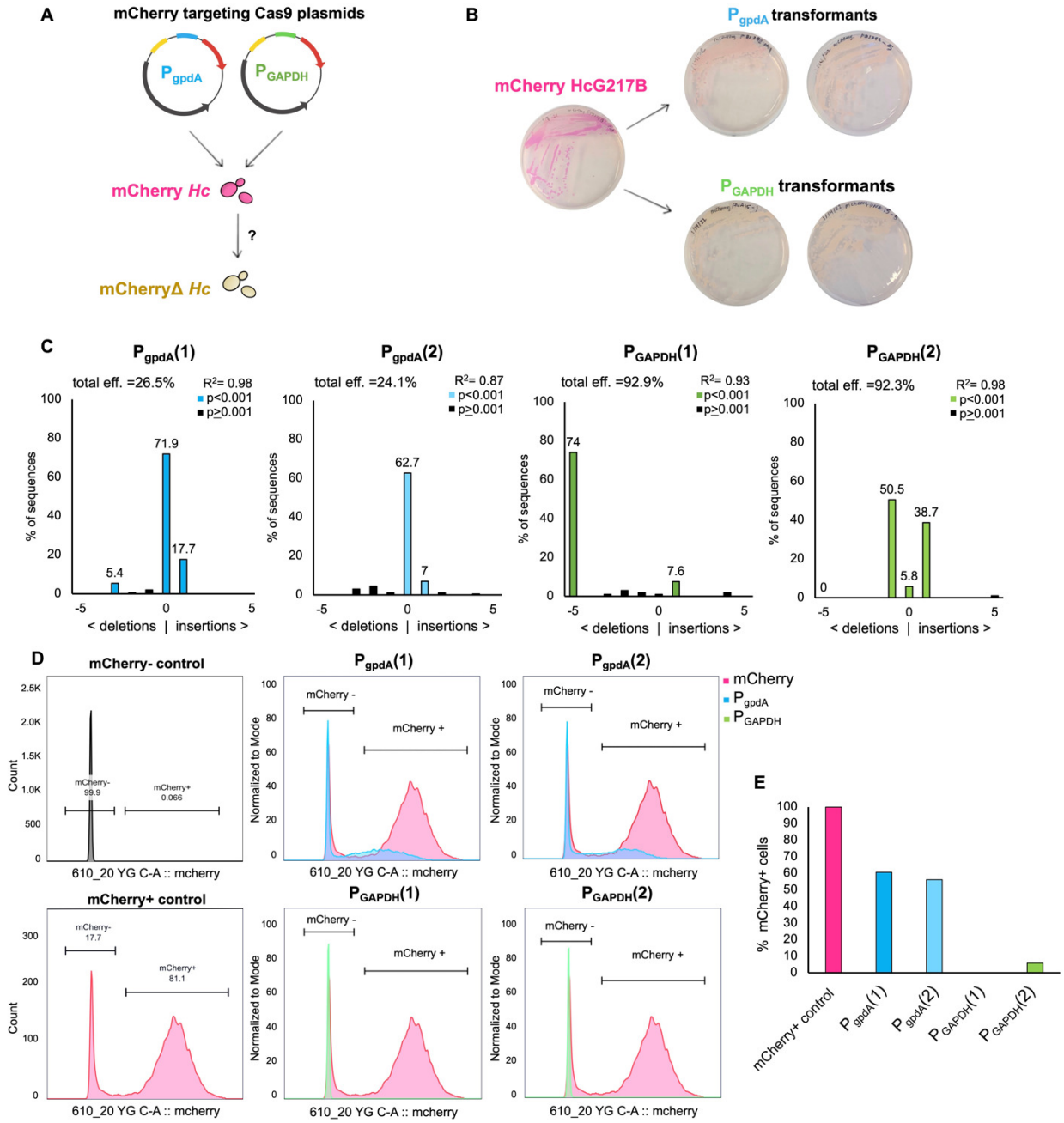

Figure 7. Cas9-sgRNAs expressed under the control of the *Histoplasma* GAPDH promoter showed increased editing efficiency. A) Schematic displaying experimental approach. Plasmids containing either the *A. nidulans* GAPDH promoter adapted from Nødvig et al. 2015 (P_{gpdA}) or the native *Histoplasma* GAPDH promoter (P_{GAPDH}) driving the expression of an identical mCherry targeting guide RNA were transformed into the mCherryHcG217B strain and used to assess differences in editing efficiencies. B) Plate images of the parental mCherryHcG217B strain alongside transformants selected from each plasmid transformation that were subsequently

used for Sanger sequencing and flow cytometry. C) Indel spectrum of two individual isolates obtained from each plasmid transformation. Sanger sequencing of the mCherry locus was used to conduct TIDE analysis (https://tide.nki.nl/) to quantify the frequency of insertions and deletions following the predicted cut site. D) Histograms displaying measurements of mCherry signal acquired through flow cytometry. Overlay plots display normalized counts for each isolate in comparison to the starting mCherryHcG217B strain. E) Quantification of flow data displaying percentage of mCherry+ cells within each isolate.